Solar Energy Materials & Solar Cells 230 (2021) 111209

Contents lists available at ScienceDirect

Solar Energy Materials and Solar Cells

journal homepage: www.elsevier.com/locate/solmat

# Experimental development and testing of low-cost scalable radiative cooling materials for building applications

Laura Carlosena [a,b,c,*], Ángel Andueza [d,e], Luis Torres [c], Olatz Irulegi [b], Rufino J. Hernández-Minguillón [b,c], Joaquín Sevilla [d,e], Mattheos Santamouris [f]

[a] Department of Engineering, Universidad Pública de Navarra, Campus de Arrosadía-31006, Pamplona, Navarra, Spain
[b] Architecture Department, University of the Basque Country UPV/EHU, Plaza Oñati 2, 20018, San Sebastian, Spain
[c] Alonso Hernández & Asociados Arquitectura S.L., 31006, Pamplona, Spain
[d] Department of Electrical, Electronic and Communications Engineering, Universidad Pública de Navarra, Campus de Arrosadía-31006, Pamplona, Navarra, Spain
[e] Smart Cities Institute (SCI), Universidad Pública de Navarra, Campus de Arrosadía-31006, Pamplona, Navarra, Spain
[f] The Anita Lawrence Chair of High Performance Architecture, University of New South Wales, Sydney, NSW, 2052, Australia

ARTICLE INFO

*Keywords:*
Daytime radiative cooling
Spectrally selective materials
Scalable material development
Subambient cooling
Spray coating deposition

ABSTRACT

Urban overheating has a serious impact on building energy consumption. Daytime radiative cooling materials are an interesting passive solution for refrigeration. However, their costs and complex manufacturing hinder their current application. In this study, a series of scalable and lowcost daytime radiative cooling (DTRC) materials were designed, fabricated, and tested in a moderate climate (Cfb-Köppen-Geiger classification) and compared to aluminum and Vikuiti. The methodology was: i) material selection and design, (ii) optimization, (iii) fabrication, (iv) characterization, and (v) testing. The materials were fabricated using different substrates, aluminum and Vikuiti, and two kinds of formulations for the emissive layers based on silica-derived polymer polymethylsilsesquioxane (PMSQ) with embedded silica nanoparticles. The resulting aluminum DTRC materials had a mean solar reflectivity of 0.7 and 0.34 emissivity in the atmospheric window, the samples with Vikuiti had 0.97 and 0.89, respectively. During the experiment, the samples were exposed to different ambient conditions without a convection barrier and were contained in an extruded polystyrene board to eliminate conduction. The samples reached 7.32 °C and 9.13 °C maximum surface temperature reduction (below ambient) during the day and night, respectively. The samples with the commercial substrate achieved a mean reduction of 3.72 °C below ambient temperature. Although the aluminum samples did not achieve subambient cooling throughout the entire day, the emissive layer reduced the sample's surface temperature by an average of 1.7 °C. The PMSQ radiative cooling materials show great potential for future building applications. Suitability under different climates and experimental settings should be done to test broad applicability.

## 1. Introduction

Urban heat islands are the most documented phenomena of climate change. Urban overheating is associated with higher urban temperatures in the dense parts of the cities compared to the surrounding suburban or rural areas [1]. Overheating sources include the released anthropogenic heat, high absorption of solar radiation by the urban materials and structures, decreased airflow and urban ventilation, reduced evapotranspiration, and limited radiative losses [2]. The phenomenon is documented in more than 400 cities worldwide; the amplitude of urban overheating may range between 1 and 10 °C averaging 5 to 6 °C [3]. Synergies with the global climate change and heat waves further intensify the amplitude of urban overheating [4].

Urban overheating has a serious impact on the cooling energy consumption of buildings, outdoor pollution levels, heat related mortality and morbidity, urban ecological footprint and survivability levels [5]. It is reported that urban overheating rises the peak electricity load varies between 0.45% and 4.6%, equivalent to an electricity penalty of about 21 (±10.4) W per degree of temperature increase and per person [6]. Moreover, the additional energy penalty induced by urban overheating is close to 0.74 kWh/m$^2$/C, while the Global Energy Penalty per person is close to 237, (±130) kWh/p [7]. In parallel, recent research has found

* Corresponding author. Department of Engineering, Universidad Pública de Navarra, Campus de Arrosadía-31006, Pamplona, Navarra, Spain.
*E-mail address:* laura.carlosena@unavarra.es (L. Carlosena).

https://doi.org/10.1016/j.solmat.2021.111209
Received 11 February 2021; Received in revised form 22 April 2021; Accepted 27 May 2021
Available online 11 June 2021
0927-0248/© 2021 The Authors. Published by Elsevier B.V. This is an open access article under the CC BY-NC-ND license (http://creativecommons.org/licenses/by-nc-nd/4.0/).

that populations living in cities' with warmer precincts have a close to 6% higher risk of mortality than those living in cooler urban neighborhoods [8].

To counterbalance the impact of urban overheating, several mitigation technologies have been proposed and implemented in cities. Proposed technologies include reflective and chromic materials for the urban fabric, additional green infrastructure, evaporative systems, solar control devices, and the use of low temperature heat sinks [3]. Implementation of the proposed mitigation technologies in large scale projects showed that it is possible to decrease the peak temperature of cities up to 2.5–3 °C [9]. Among the various proposed technologies, the use of reflective, thermochromic, and photonic materials seems to present the highest mitigation potential [10]. Recent data have shown that the use of reflective materials in cities reduces the ambient temperature by 0.09 °C per 0.1 increase of the urban albedo while reducing heat related mortality between 0.1 and 4 deaths per day [11].

The recent development of photonic and plasmonic materials has skyrocketed the mitigation potential of modern materials used in the built environment. Photonic materials or Daytime Radiative Coolers (DTRC) exhibit subambient surface temperatures during the daytime under the sun [12].

Daytime radiative cooling materials can be classified into multilayer photonic structures, metamaterial 2D-3D photonic structures, polymers, and paints for radiative cooling [12]. Although other materials had previously achieved daytime radiative cooling, a new photonic material recently reached 4 °C below ambient temperature under direct sunlight [13]. This photonic material was a breakthrough in the field, and many authors have followed their approach. Numerical simulation of the sample inside a vacuum chamber showed a theoretical maximum reduction of 60 °C [14] below ambient temperature. Experimentally, the material achieved an average temperature reduction of 37.4 °C with a sunblock. A double-layer coating composed of densely packed titanium dioxide particles on top of densely packed silicon dioxide or carbide nanoparticles can theoretically achieve 17 °C below ambient at night and 5 °C below ambient under direct solar radiation. However, experiments conducted in Shanghai did not achieve subambient temperatures due to high relative humidity [15]. A polymer-coated fused (PDMS) silica mirror achieved radiative cooling below ambient air temperature under direct sunlight of 8.2 °C [16]. Using periodic high and low index layers a radiative cooling power of 100 W $m^{-2}$ was attained [17]. An optimized BN, SiC, and $SiO_2$ gratings on top of a metal/dielectric multilayer structure reached a mean cooling power of 55 W $m^{-2}$ [18]. An equilibrium daytime temperature of −13 °C and a cooling power of 105 W $m^{-2}$ was achieved with two thermally emitting photonic crystal layers comprised of SiC and quartz, on top of a broadband solar reflector made of three sets of five bilayers made of $MgF_2$ and $TiO_2$ with varying periods on a silver substrate [19]. A complex structure of symmetrically shaped conical metamaterial pillars composed of alternating layers of aluminum and germanium can reach a daytime equilibrium temperature of 9 °C below the ambient temperature and 12 °C at night [20].

Photonic materials sometimes include 3D volumes to improve and tune the emissivity towards the desired spectrum. A cell consisting of a thick phosphorus-doped n-type doped silicon substrate and two identical rectangular dielectric resonators numerically achieved a nighttime minimum temperature decrease of 10.29 K at thermal equilibrium and 7.36 K at daytime with a maximum net cooling power of 95.84 W $m^{-2}$ [21]. An experiment doped 25 μm thick polyethylene (PE) with SiC and $SiO_2$ nanoparticles on top of aluminum, the device was covered with an IR transparent cover (10 μm PE) to avoid convective heat gains achieving an actual stagnation temperature of 17 °C below ambient in Sydney with about 3 mm of water vapor pressure [22].

Many radiative cooling materials have been developed using polymeric derived composites. A glass-polymer hybrid material [23] achieved a cooling power of 93 W $m^{-2}$ under direct sunshine at noon. The material's performance was tested in China comparing two boxes (one with the material and the other without it) where the inside air temperature was measured, showing a 21.6 °C difference between [24]. A cost-effective double-layer coating embedded with titanium dioxide and black carbon particles predicted a net cooling power of 100 W $m^{-2}$ during the day and 180 W $m^{-2}$ at night [25]. Another test in Shanghai compared twelve samples of $SiO_2$ microsphere-Poly-4-methyl-1-pentene (TPX) hybrid system deposited on fluorine doped tin oxide (FTO) substrates showing temperatures about 20 °C lower than a black surface, 12 °C lower than the silver coated glass, and 8 °C lower than the FTO sample; however, they did not achieve subambient cooling, showing an average temperature of 15 °C higher than ambient.

Paints for easy and scalable application based on a hierarchically porous poly (vinylidene fluoride-co-hexafluoropropene) have achieved a subambient temperature drop of 6 °C and cooling powers of 96 W $m^{-2}$ [26]. A 7.3 °C subambient temperature drop was reported at noontime in Beijing by spraying zinc phosphate sodium onto aluminum [27]. Aperture dependency designs with shaded radiative cooling surfaces were introduced by Trombe (cited by Ref. [28]) and continued by Refs. [28–31], showing temperature drops of up to 11 °C below ambient temperature.

Besides material development, several authors focused on system development [32–39]. However, systems relying solely on fluid circulations are focused on nighttime radiative cooling. A radiator insulated with polystyrene foam and bubbled plastic sheets used as top cover achieved 20 °C below ambient temperature without a heat source and a plastic cover in Shiraz (Iran) [32]. Erell and Etzion tested a system based on circulating water from a roof pond through a radiator system, the high water temperature aided in the heat elimination from radiation and convection [33]. The same authors tested a cheap, simple, and flexible design for a cooling radiator, achieving a mean nightly cooling output of 90 W $m^{-2}$ under typical desert meteorological conditions in Israel [34]. An unglazed radiator performed well in clear and low humidity nights in Norway; nevertheless, the authors [35] suggested experimenting in climates with cooling demand. Similar research conducted in Iran achieved an average net cooling power of 45 W $m^{-2}$ and lowered the water accumulation tank up to 8 °C [36]. A group of Spanish researchers tested radiators with different infrared emissivities and achieved average cooling powers of 60 W $m^{-2}$ [37].

Recent research proposed a single-phase thermosiphon [38] for cold collection and radiative cooling storage. Instead of using an electric pump, their device used buoyancy force to drive heat transfer fluid and achieved an average cooling flux of 105 W $m^{-2}$ cooling flux. A daytime radiative cooling system was proposed in Ref. [39], where series of panels cooled water up to 5 °C below the ambient air temperature, covering the panels with a visibly-reflective extruded copolymer mirror (3M Vikuiti Enhanced Solar Reflector ESR film). Moreover, the authors modeled the panel integrated on the condenser side of a building's cooling system in Las Vegas and calculated an electricity reduction of 21% during the summer.

Systems that work at temperatures higher than the ambient present an advantage since convective heat exchange increases the rate at which energy is removed from the system rather than impede it. This feature of the system obviates the need for windscreens [33]. Convective heat gains remain a problem to be solved. If subambient temperatures are reached, the convection forces tend to augment the temperature of the radiative cooler. According to Lu et al. [40], the convective heat transfer reduction can be solved in two ways, with wind covers and windshields. The most researched wind covers have been made of polyethylene [41–43]. However, its aging degradation is a challenge to be solved [44]. When a thin layer of water precipitates directly on the radiator, it improves its performance since water has a high emissivity. Nevertheless, it reduces the transmittance when it is located on the cover and, therefore, the net output thermal radiation [45]. Moreover, dust accumulation reduces the efficiency of radiator systems that incorporate transparent windscreens [33]. Finally, radiative cooling materials' optimal spectral characteristics depend on the climate conditions and the type of application [46]. In that study, a series of daytime radiative

cooling materials, theoretical materials, and existing materials were simulated under a passive and active approach in two differentiated climates, concluding that a material that performs well in a dry climate as a passive solution could perform poorly as an active solution.

This research aims to study low-cost scalable DTRC materials for the built environment under different meteorological conditions. The authors studied the performance of several materials and compared them with the substrates without coatings. The materials were tested in a moderate climate nearby Pamplona (Spain) Cfb according to the Köppen-Geiger classification without a convection shield. This research's novelty is the design, optimization, and testing −under different meteorological conditions− of innovative low-cost and scalable daytime radiative cooling materials.

## 2. Methodology

This research focuses on developing and testing scalable daytime radiative cooling materials for future application in the built environment based on a reflective substrate and an emissive layer. First, different types of multilayer materials were studied and compared as candidates to enhance the emissivity of the radiative cooling surfaces in the atmospheric transparency window for applications as built environment coatings. The design of these multilayer structures' parameters was done considering industry fabrication capabilities for film deposition, and then, the dimensions of each design were analyzed to obtain maximum absorption from 8 to 13 μm. After the materials and the structure design compositions were selected ($SiO_2$ as emissive layer and aluminum as substrate), a series of numerical optimizations were made to determine each layer's ideal thickness. Secondly, a systematic process based on computer simulation using the CST Studio Suite [47], a commercial code based on the Finite Integration time-domain Technique (FIT), was developed to determine the emissivity response of the analyzed samples. Moreover, the optical response in the visible range was simultaneously calculated and analyzed to evaluate the proposed structures' effect in the reflected and transmitted power. Afterward, the materials were fabricated and characterized in the visible and infrared wavelengths. Finally, the samples were tested under non-ideal outdoor conditions.

### 2.1. Material selection and design

The research takes after the approach proposed in Refs. [48,49], which includes a reflective substrate and an emissive coating. Therefore, the selected materials for optimization are silica and aluminum. Silica is transparent in the visible range presenting a refractive index almost constant of 1.4. The transmittance of silica is high until 2.5 μm; from that wavelength onwards, silica is almost opaque, its absorption rises strongly, and the transmitted power can be considered zero. Therefore, silica presents a significantly different refractive index in the visible region and the atmospheric window (AW) (8–13 μm), influenced by the vibrational modes of oxygen atoms [55]. The excitation of these vibrational modes by infrared (IR) radiation is macroscopically observed as absorption bands in the IR spectrum at 9 and 20 μm [57].

When calculating a silica layer's absorption, we find two different situations depending on the layer thickness. When the layer thickness is greater than the incident wavelength, most of the energy is absorbed by the material at the atmospheric window wavelengths. However, silica layers with a thickness smaller than the IR light wavelength transmit radiation for all wavelengths except for the abovementioned bands. Therefore, strong absorption is obtained using thin silica layers in narrow spectral regions centered at 9 and 20 μm.

Aluminum reflectance is higher than 90% from near UV to mid-IR except for a sharp dip at 0.8 μm. The best reflectance aluminum performance is obtained from mid-IR (2 μm), making it an excellent lossy reflector in the thermal wavelength range. Aluminum slowly oxidizes, resulting in a reduction of reflectance. Therefore, aluminum must include a protective dielectric overcoat that prevents oxidation.

### 2.2. Optimization

The design parameters of these multilayer structures were chosen considering industry fabrication capabilities for film deposition. Each design's dimensions were analyzed to obtain maximum absorption in the AW (8–13 μm). A systematic process based on computer simulation was developed to determine the analyzed samples' emissivity/absorptivity response. Moreover, the optical response in the visible range was simultaneously calculated and analyzed to evaluate the proposed structures' effect in the reflected and transmitted power. The target was to obtain the highest reflectivity in the solar wavelengths and the highest emissivity possible in the atmospheric window. Simulations in the thermal wavelength range (8–13 μm) were carried out using the CST Studio Suite, based on FIT [50]. FIT is a consistent discretization scheme that provides a reformulation of Maxwell's equations in their integral form suitable for computers, and allows to simulate electromagnetic field problems with complex geometries and materials. This program is an electromagnetic field simulation software package especially suited for analysis and design in the microwave, terahertz, and optical range.

In order to calculate the absorptivity of the structures in the visible and the near IR (NIR) ranges, we used Grating Diffraction Calculator (GD-Calc) code [51], a commercial software package developed by Kenneth C. Johnson and integrated into Matlab that uses rigorously coupled-wave analysis (RCWA) [52]. GD-Calc resolves the Maxwell equations for a single frequency and analyzes the weight of each diffraction order separately in the power balance. A summation of the power density in all diffraction orders provides the reflection and transmission values, obtaining the absorption. GD-Calc's properties resolve the meshing problems in the visible range of CST for large-sized samples since it is possible to simulate structures much larger than the shorter wavelength of the calculation in a reasonable period [53].

The composition of aluminum with an emissive layer of $SiO_2$ was simulated. As is shown in Fig. 1, the thicker the silica coating is, the more emissive it is in the AW. On the other hand, the increasing thickness does not increase the emissivity on the solar wavelengths.

A layer of silver was included to improve the reflectivity in the solar wavelength range. Two thickness values were simulated, 100 nm and 200 nm. The result in Fig. 2, compares the reflectivity with the same structure without the silver coating. Both silver thicknesses result in the same optical behavior (dashed grey line and solid red line are identical). As shown in the figure, the material without the silver coating (solid black line) is less reflective in the solar wavelengths and its average emissivity is higher without silver. Moreover, the emissivity is significantly reduced from 0.5 μm onwards using a silver layer, enhancing the

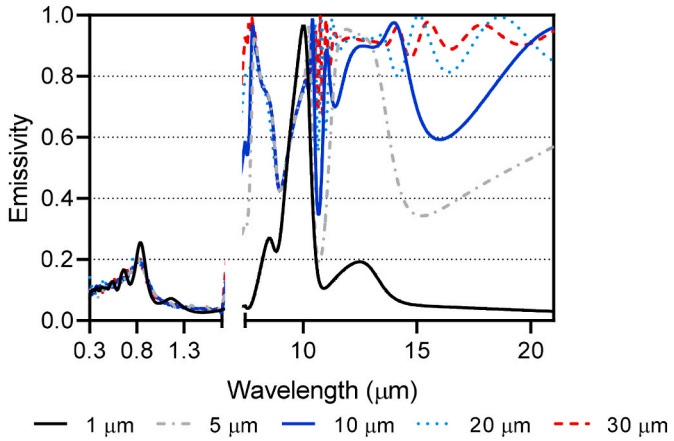


**Fig. 1.** Radiative cooling material: emissivity calculations for aluminum with different thicknesses of $SiO_2$.

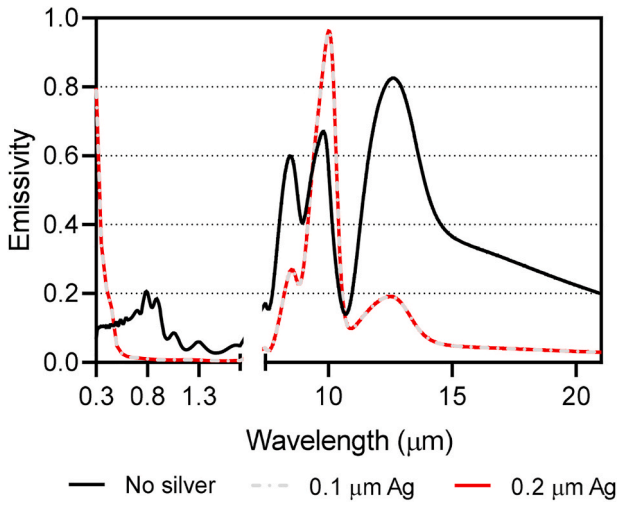


**Fig. 2.** Emissivity simulation of an aluminum substrate with different thicknesses of silver and 2 μm of $SiO_2$: no silver (solid black line), 0.1 μm (dashed grey line), and 0.2 μm (solid red line). (For interpretation of the references to colour in this figure legend, the reader is referred to the Web version of this article.)

range's reflectivity.

### 2.3. Development

Several deposition technique options were researched, such as plasma-enhanced chemical vapor deposition (PECVD) and sputtering; however, since the deposition's scalability was a requisite, spray coating was chosen. As a result of choosing this deposition method, instead of working with $SiO_2$ as a bulk material, a silica derived polymer, polymethylsilsesquioxane (PMSQ), was chosen to be applied on the substrate. The simulation study established the importance of having two layers (reflective and absorptive) and the required thickness's magnitude to obtain their optimal characteristics.

The emissive layer was fabricated by L'Urederra Technological Center using 20 nm silica $SiO_2$ nanoparticles embedded at a 5% weight in a PMSQ matrix. The aluminum substrate finish was a mirror polished, alloy 1050A H18, which is the most reflective on the market. Nevertheless, once its reflectivity was measured, it was lower than the theoretical maximum (Fig. 3). Therefore, 3M Vikuiti Enhanced Solar Reflector [54] was an alternative substrate to aluminum, used previously in two works [39,55]. As seen in Fig. 2, adding a nanolayer of silver would increase its solar reflectivity; however, it would lead to higher costs and scalability and therefore was dismissed.

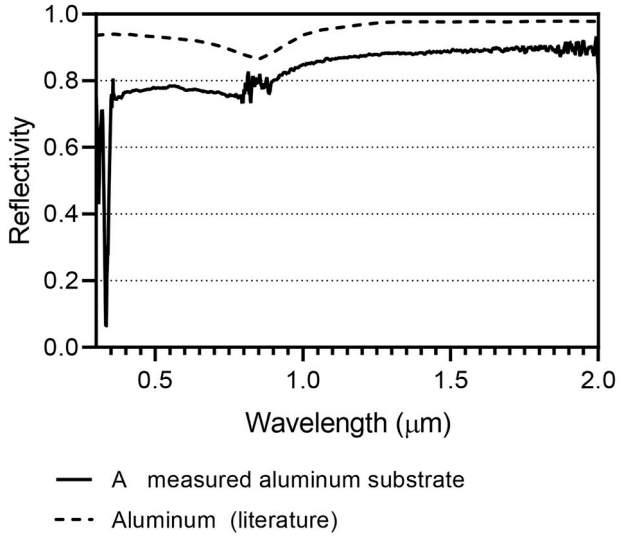


**Fig. 3.** Solar reflectivity simulation of the aluminum substrate (solid black line) vs. theoretical aluminum (dashed black line) [56].

Although the final product differed from the one designed and optimized in subsection 2.2, unfortunately, no new optimizations could be carried out since the emissive layer's exact complex refractive index is a prerequisite for simulating. To measure the refractive index, several universities and research centers were contacted. However, they could not characterize the complex index due to the impossibility of measuring rough samples in the mid-infrared (2–20 μm). The refractive index measurement requires perfectly planar specular surfaces and is usually measured with an ellipsometer from 200 to 1500 nm and a spectrophotometer for the infrared. If the samples are rough, as in this case, complex models specifically developed are used and require several different measurements (diffuse reflectance in the solid sample and powder absorption). The second alternative to optimize the thickness was to use information from the literature, but the complex index of PMSQ was not available in the literature as far as the authors know. Hence, the materials could not be optimized with the real refractive indexes.

The samples were developed using spray deposition on top of squares samples of 200 by 200 mm of two different materials: aluminum and Vikuiti ESR films (Fig. 4). The substrates were washed with ethanol paper to clean the surface from impurities, allowing a correct deposition of the emissive layer. Depending on the substrate's nature, metallic or plastic, two different emissive layers were applied (Fig. 5) (see the resulting samples in Fig. 8).

The metallic samples were curated for an hour on a stove at 200 °C. Nevertheless, the samples with a plastic substrate did not have a post-application treatment, and the emissive layer was curated at ambient temperature. The aluminum samples were applied changing the deposition speed and quantity to achieve a layer of approximately 1 μm. Target thickness was 10 μm, but due to viscosity restrictions of deposition, the maximum deposited thickness was 3.7 μm. The Vikuiti substrates received two and three layers of the emissive coating to achieve the minimum 1 μm target.

### 2.4. Characterization

The reflectance was characterized in the visible and near-infrared spectra (from 200 to 1100 nm), using a combined Deuterium Halogen light source (Top Sensor System DH-2000-S) with an integrating sphere and a CCD spectrometer (OceanOptics USB2000-FLG) with an unpolarized light source and a calibrated high specular reflectance standard. A Fourier transform infrared spectrometer (Bruker Vertex 80V)

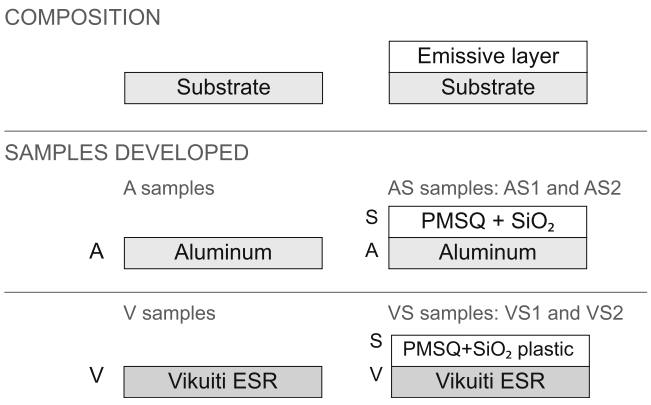


**Fig. 4.** Configuration of the different fabricated samples. A stands for the aluminum substrate, AS for the aluminum plus the emissive layer, V for Vikuiti, and VS for Vikuiti plus the emissive layer.

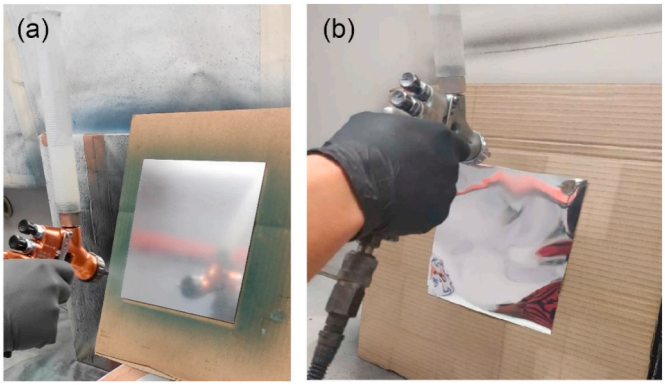


**Fig. 5.** Spray coating onto (a) metallic substrate and (b) plastic substrate.

equipped with an infrared microscope (Hyperion 3000) was employed to perform measurements in the near-infrared (NIR, 0.78–2.5 μm) and mid-infrared (MIR, 2.5–25 μm). The excitation was done with unpolarized light sources (halogen lamp in the NIR and a Globar source in the MIR) and the detection with an InGaAs detector (NIR) and a nitrogen cooled MCT detector (MIR). The cooler's reflectance was characterized in normal reflection with a gold mirror used as a reflectance standard. Besides the emissivity and reflectivity measurements, all samples had their coating thickness, adherence, gloss, and hardness characterized.

### 2.5. Experimental setup

The performance of the materials was compared to the substrates without any coating. The samples were contained in hollowed-out squares in an extruded polystyrene (XPS) board to eliminate heat conduction; this condition can be considered almost adiabatic. The experiment was conducted from October 16 to 20 of 2020 (Day 1 to Day 5) on the National Renewable Energy Center (CENER) rooftop, as is shown in Fig. 6. Meteorological data was recorded using CENER's equipment throughout the duration of the experiment. The station is composed of 3 pyranometers for global horizontal irradiance (Kipp&Zonen, CMP22), 1 shaded pyranometer for diffuse radiance (Kipp&Zonnen, CMP22), 1 pyrheliometer on a sun tracker for beam irradiance (Kipp&Zonnen, CHP1), and a shaded pyrgeometer for downwelling infrared radiation (Kipp&Zonen, CGR4). Kipp & Zonen equipment maximum uncertainty is 2% for hourly totals and 1% for daily totals. Other components are sensors to measure atmospheric pressure (Vaisala, PTB110), air temperature and relative humidity (Vaisala, HMP45C), and wind speed with an anemometer (Ammonit, P6100H). The air temperature measurements range from −39.2 °C to +60 °C, the accuracy at 20 °C is ±0.2 °C. The relative humidity measurement range is 0.8–100 °C with accuracy at 20 °C against factory references ±1 %RH. The anemometer range is 0.3–75 $ms^{-1,}$ and ±0.03 $ms^{-1}$ accuracy, and the wind vane has a full 360° range, ± 2° accuracy, and 0.5° resolution.

This data was used to characterize the outdoor climatic conditions onsite. The measurement is based on the thermal balance of the material. The surface temperature when exposed to the direct sun complemented with the meteorological data is needed for testing material's thermal performance. The six samples' surface temperature was monitored with six surface temperature sensors (thermocouples type K connector TP from Testo) connected to 3 data logging devices (Testo Saveris 2-T3 WiFi) with ± (0.5 + 0.5% of mv) °C accuracy and range is −40 °C–400 °C with ±0.2 °C accuracy. As seen in Fig. 7, a cell phone connected to a battery was placed to generate a WiFi net to retrieve data from the dataloggers and synchronize it with the cloud.

The following equations describe the experiment's thermal balance.

$$P_{out} = \varepsilon_s \cdot \sigma \cdot T_{sample}^4 \tag{1}$$

where $P_{out}$ is the outgoing radiating power $\varepsilon_s$ *is* the emissivity of the surface the blackbody radiation in the wavenumber $\nu$ when its temperature is $T_s$, $G_s(\nu)$ the irradiance received by the surface at a wavenumber $\nu$.

$$P_{in} = R_{solar} + (h_{conv} + h_{cond}) \cdot \left(T_{amb} - T_{sample}\right) + R_{amb} \tag{2}$$

$$\Delta T = (\mathrm{P_{in}} - P_{out}) / A_{surface} \tag{3}$$

## 3. Results

### 3.1. Samples and characterization

Two types of radiative cooling materials were developed, based on an aluminum metallic substrate and a plastic substrate, summarized in Table 1 and shown in Fig. 8. The following samples were tested, a bare aluminum substrate (A), the Vikuti sample (V), 2 DTRC materials of aluminum with the silica emissive layer (AS1 and AS2), and 2 two samples of the emissive layer formulated for plastic deposition on top of a Vikuiti film (VS1 and VS2).

As shown in Fig. 9(a) and Fig. 10(a), the reflectivity in the samples' optical range with aluminum and Vikuiti ESR substrates is significantly different. The commercial substrate (Vikuiti) presents a reflectivity close to 1 for all the analyzed samples, including the samples with the

**Fig. 6.** Photos of the experimental setup in CENER, Sarriguren, Spain. The samples are contained in an XPS board and monitored with thermocouples connected to dataloggers.

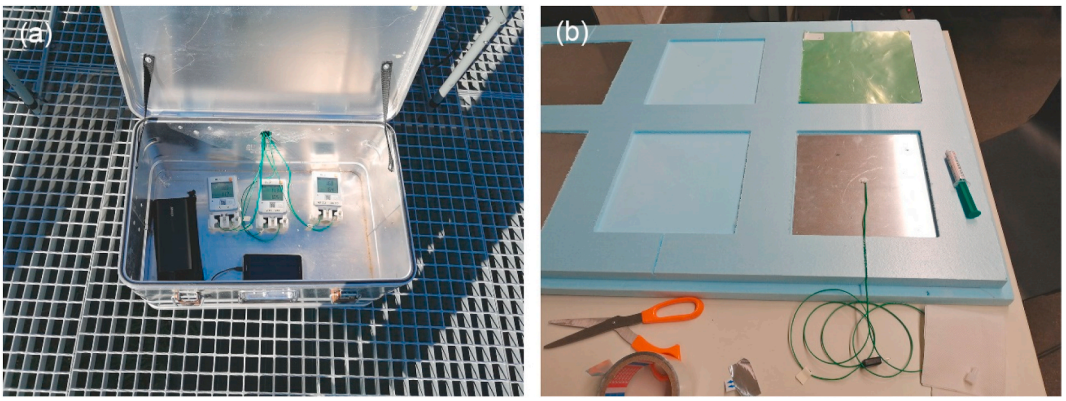


**Fig. 7.** Photos of the experimental setup (a) 3 WI-FI dataloggers (2 thermocouples each), Wi-Fi-net created with a smartphone plugged into a power bank to allow remote monitoring during several days, (b) the thermocouple is attached with thermal paste to the samples' bottom side with conductive paste.

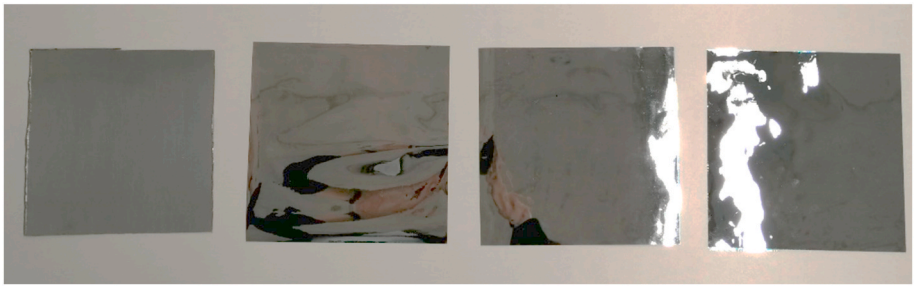

**Fig. 8.** Photo of the samples indicated in Table 1, from left to right: aluminum with an emissive coating (AS1), Vikuiti Substrate (V), and two samples with the emissive layer on Vikuiti ESR (VS1 and VS2).

**Table 1**
Summary of the developed samples. S stands for substrates and DTRC for Daytime Radiative cooling materials. A is the aluminum substrate, AS the aluminum plus the emissive layer, V is Vikuiti, and VS is the Vikuiti substrate plus the emissive layer.

| | | Substrate | Emissive layer | | |
|---|---|---|---|---|---|
| | Sample code | Material | Material | Thickness | Mass |
| S | A | Al (1 mm) | – | – | – |
| | V | Vikuiti ESR | – | – | – |
| DTRC | AS1 | Al (1 mm) | PMSQ + nanoparticles | 1.5 ± 0.6 μm | 13.3 mg |
| | AS2 | | $SiO_2$ | 2.2 ± 0.4 μm | 22.5 mg |
| | VS1 | Vikuiti ESR | Plastic PMSQ + nanoparticles | – | 17.4 mg |
| | VS2 | | $SiO_2$ | | 36.6 mg |

emissive layer. In contrast, the aluminum substrate shows a reflectivity of 0.7, 30% lower than Vikuiti, lowering up to 0.6 when the emissive coating is applied (Fig. 9(a), red solid and blue dashed lines). The previous result suggests that emissivity increased, as shown in Fig. 9 (b), from 0.3 to 0.4. On the other hand, observing the coatings' effect in the atmospheric window (Figs. 9(b) and Figure 10(b)), coating increases the total emissivity in the range 8–13 μm for both cases. The emissive coat (Fig. 9(b)) enhances the emissivity at 10 μm from 0.04 to 0.45 and 0.7 for the samples AS1 and AS2, respectively. It is important to note that the abovementioned emissivity peak appears by the effect of the silica particles. In the atmospheric window, A shows 3.3% emissivity; the application of the coating increases the emissivity value by 24% for AS1 and 32.9% for AS2. In V's case, the AW's emissivity is 85.8% increasing by 9% for VS1 and 1% for VS2. This result agrees with the numerical calculations of silica films with a thickness of around 1 μm shown in Fig. 1. The simulations' main differences are especially significant in the emissivity value at 13 μm wavelength due to the PMSQ matrix where the silica particles are embedded (Fig. 11). In the case of Vikuiti ESR substrate, the effect of the PMSQ enhances emissivity by 10% in the IR range compared to the bare sample. In contrast, the layer's effect is almost constant from 1 to 17 μm obtaining a broadband emissivity response.

As mentioned before in 2.3, the simulations and optimizations were conducted with ideal and bulk materials, whose refractive indexes were obtained from databases and literature. The differences between simulated and measured emissivity are due to the final materials used. A silica derived polymer, PMSQ, was employed instead of using bulk $SiO_2$ films. Which has a different effective refractive index from silica. Nevertheless, the simulations validated the proposed structure and gave a better understanding of the structures' optical behavior. Moreover, they provided useful information regarding the appropriate emissive material's thickness.

As mentioned above, a comprehensive characterization was performed, where the samples' reflectivity and emissivity, the coating thickness, hardness, and gloss were measured, as seen in Table 2. Once the emissive coating was applied to the aluminum samples, the gloss was reduced significantly. On the contrary, little difference was seen in the Vikuiti samples.

The proposed emissive layer has an approximate cost of 0.3 €/$m^2$ for a layer of 2 μm of PMSQ and $SiO_2$ nanoparticles, being competitive for built-environment applications.

### 3.2. Experiment

The experiment conducted in the National Renewable Energy Center (CENER) rooftop allowed the samples' direct exposure to the sky without unobstructed views since the facility is designed to test solar

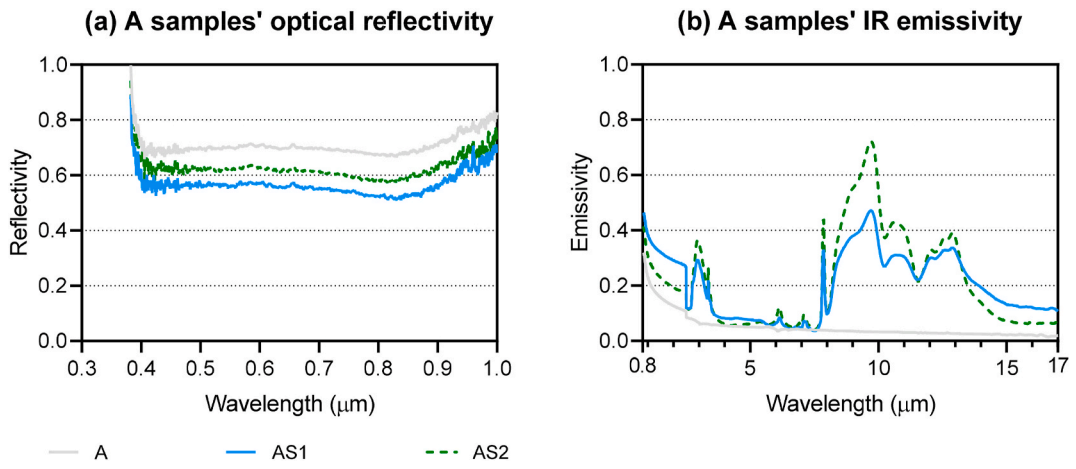


**Fig. 9.** Measured (a) optical reflectivity and (b) IR Emissivity of the samples with aluminum substrate (A), and two samples of aluminum with emissive coating, AS1 and AS2.

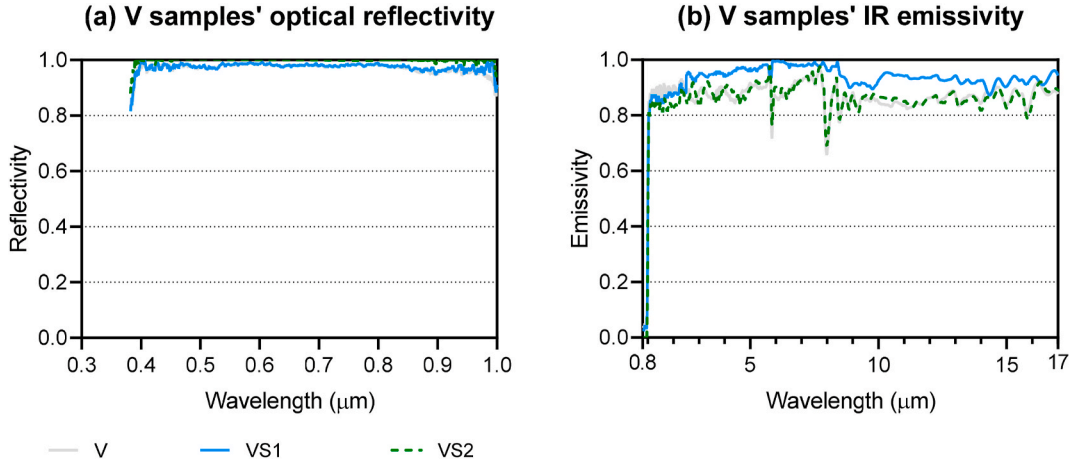


**Fig. 10.** Measured (a) optical reflectivity and (b) IR Emissivity of the samples with Vikuiti ESR substrate (V), V bare Vikuiti substrate, and two samples with emissive coating, VS1 and VS2.

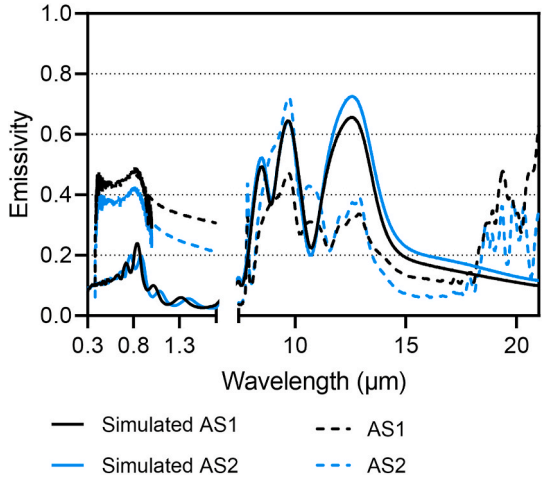


**Fig. 11.** Emissivity comparison between the developed aluminum and PMSQ samples (AS1 and AS2) and the simulated aluminum and $SiO_2$ samples (Simulated AS).

**Table 2**
Sample's characterization: gloss, hardness, and the number of layers of emissive coatings.

| | Sample code | Gloss 60° | Hardness | Number of layers of emissive coating |
|---|---|---|---|---|
| S | A | 721 ± 6 | <9B | – |
| | V | 1001 ± 2 | – | – |
| DTRC | AS1 | 437 ± 23 | H | 1 layer slow speed application |
| | AS2 | 465 ± 34 | F | 2 layers regular speed application |
| | VS1 | 997 ± 7 | – | 2 |
| | VS1 | 992 ± 4 | – | 3 |

photovoltaic and thermal panels (Fig. 12). A total of 6 samples from Table 1 were tested, the bare aluminum substrate (A), the Vikuti sample (V), 2 DTRC materials of aluminum with the silica emissive layer (AS1 and AS2), and 2 two samples the emissive layer formulated for plastic deposition on top of a Vikuiti film (VS1 and VS2). The experiment was monitored for five consecutive days with different meteorological conditions. Fig. 13 shows the meteorological data from those five days.

The samples' surface temperature was recorded and compared to the ambient air temperature in Fig. 14. By noon, all the samples achieved subambient cooling even with an incident solar radiation of 633 W $m^{-2}$


**Fig. 12.** Photos of the experimental setup, (a) Day 1: sunny day, and (b) Day 5: rainy day.

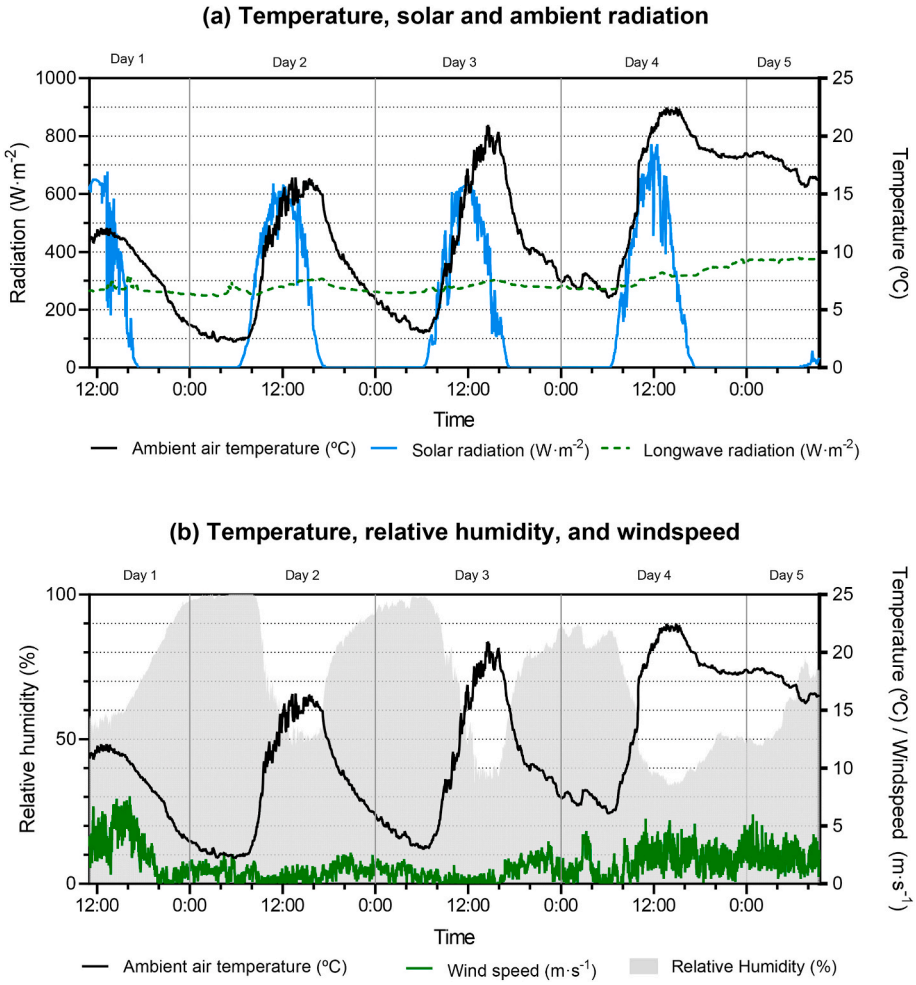


**Fig. 13.** Climate data during the five consecutive days of the experiment.

and infrared atmospheric radiation ranging from 280 to 320 W $m^{-2}$. The higher ambient temperatures induced by the solar radiation heated the samples. Before noon, the aluminum sample A was up to 3.62 °C below ambient, the samples with the emissive coating, AS1 and AS2, achieved 3.62 °C and 3.92 °C, respectively. The samples with the commercial substrate, V, V1, and V2, had a higher solar reflectivity and achieved 6.12 °C, 7.32 °C, and 7.12 °C below ambient temperature. From 12:55 onwards, the samples with the aluminum substrate were hotter than the ambient air temperature due to the high absorption of solar radiation in the 0.3–2 μm range. Nevertheless, the AS samples were up to 5 °C cooler than the aluminum sample and an average of 1 °C lower than the sample without coating. The materials with coating showed a better behavior due their ability to radiate heat in the infrared wavelengths. The Vikuiti samples' low surface temperature led to surface water condensations, as seen in Fig. 16. These samples had an almost ideal solar reflectivity and a broadband emissivity in the infrared wavelengths since the materials reflected all the incident heat and emitted any possible heat gains, leading to substantial temperature drops.

The materials presented three distinct behaviors (Fig. 13) corresponding to different climatic conditions (Fig. 14). Day 1 was sunny with

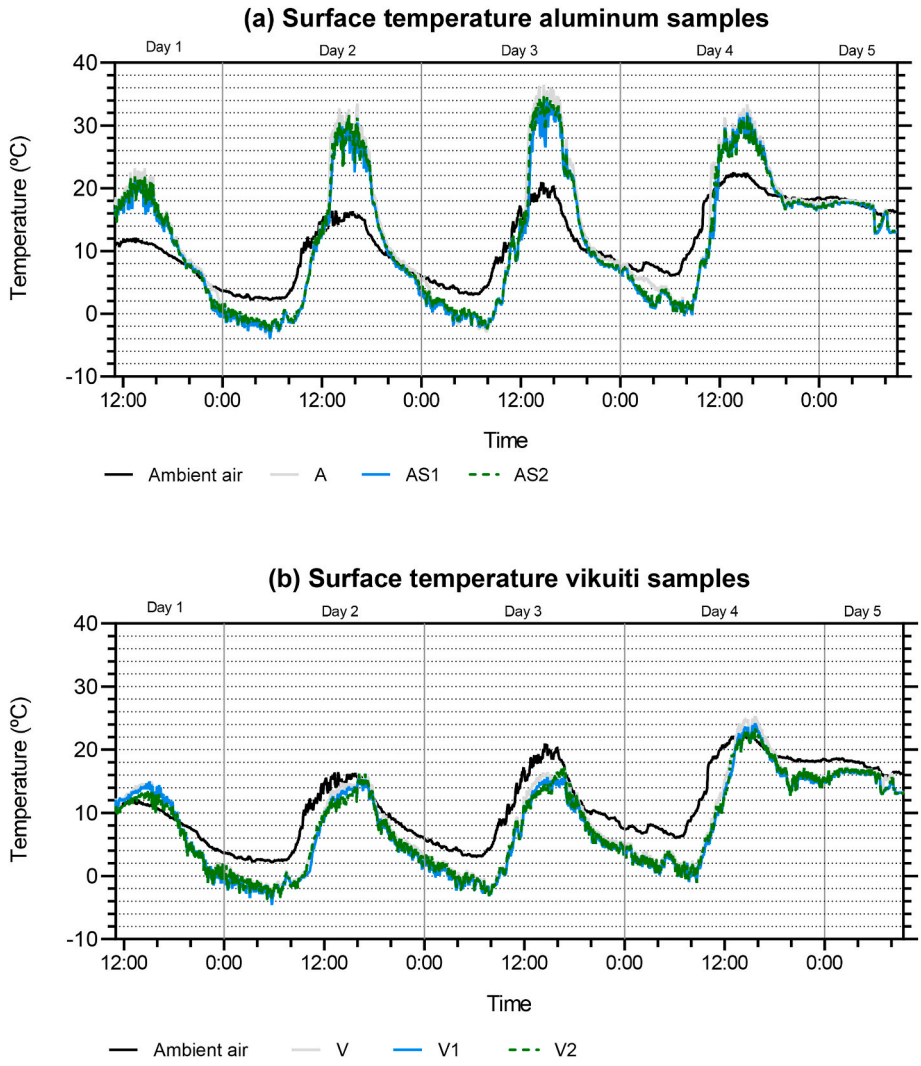


**Fig. 14.** Samples surface temperature throughout the five days of the experiment.

low temperature (mean of 10.5 °C day and 4 °C at night) and high humidity (62%), the aluminum samples heated up during the day and attained subambient cooling at night; the same happened with the V samples. The aluminum samples behaved better than on any other day, as discussed in Ref. [57], the cooling performance of the materials has an almost linear response to changes in the ambient air temperature.

Day 2 and 3 were similar, sunny with high passing clouds, moderate daytime temperature (mean of 15 °C day and 7 °C at night), medium relative humidity (55%) and low wind speeds (0.78 m $s^{-1}$); as a result, all the samples had a similar thermal response both days. Day 2 had a slightly higher relative humidity than day 3, translated into lower temperatures during day 2 and higher during day 3. The aluminum samples heated up more significantly than the previous days due to higher temperatures and similar relative humidity. The plastic samples achieved subambient cooling during both days (Fig. 14 (b)) since the relatively low humidity favors the thermal exchange. In cloudy days, broadband emitters end up absorbing radiation coming from the clouds, and as a result, the thermal equilibrium is achieved at higher temperatures.

Finally, day 4 was very sunny during daytime and very cloudy at night with high temperatures, 20.6 °C during the day and 18 °C at night, and low relative humidity (39%) and higher ambient radiation (323 W $m^{-2}$). Although the temperatures reached up to 22.3 °C during the day and were higher than the previous days, the aluminum samples were cooler, 9 °C (AS1 and AS2) over ambient temperature. Outgoing radiation evacuated from the materials was favored by low relative humidity. On the contrary, in the previous days, as seen in Fig. 14 (a), AS1 and AS2 had reached 18 °C above ambient (day 2 and day 3) since water vapor inhibits outgoing radiation. The V samples achieved higher temperatures than in the previous days and surpassed ambient temperature. This phenomenon might be explained because the longwave radiation increases from noon onwards and lower wind speeds, making the convective heat exchange lower, penalizing the broadband emitters (VS1 and VS2) while benefitting the strictly spectrally selective materials (AS1 and AS2). When surfaces are above ambient air temperature, wind helps to reduce the surface temperature. The night leading to day 5 was cloudy with higher longwave radiation (Fig. 13 (a)); thus, the samples did not cool down as much as in the previous days. Moreover, on day 4, higher convection led the Vikuiti samples below ambient air temperature to increase their temperature around and above ambient air temperature.

Finally, to see the emissive coating effect, the samples' surface temperature was compared to the bare substrate in Fig. 15. Although AS1 had a lower solar reflectivity and lower emissivity in the transparency window than AS2 (see Fig. 9), which is considered a worse optical behavior, it performed better throughout all the days, as seen in Fig. 15 (a). This behavior might be related to high relative humidity values. V samples are broadband emitters in the infrared wavelengths (Fig. 10), V and V2 had a very similar response, and V1 emissivity was higher. Nevertheless, V2 achieved more punctual temperature drops

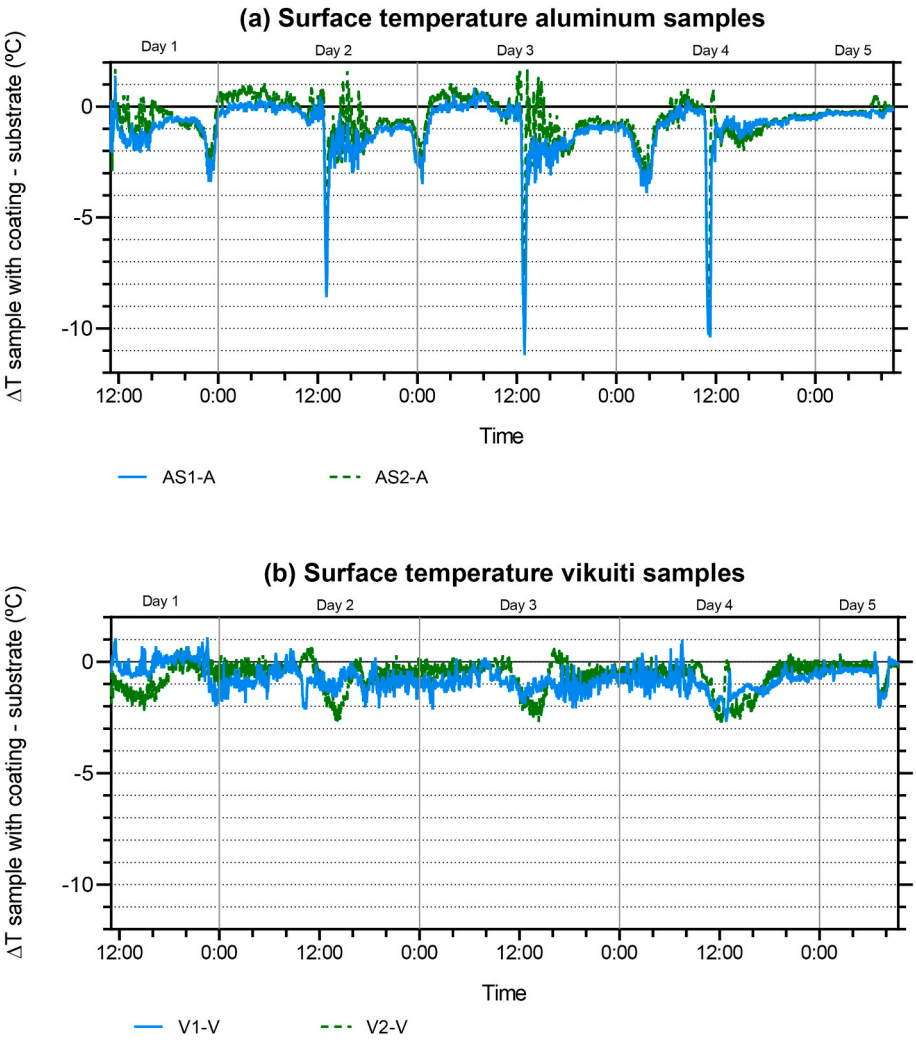


**Fig. 15.** DTRC sample's surface temperature difference with the bare substrates (a) comparison of AS1 and AS2 with bare aluminum (A) (b) comparison of V1 and V2 with bare Vikuiti substrate (V). Negative values reflect when the samples with coating are below the substrate's temperature.

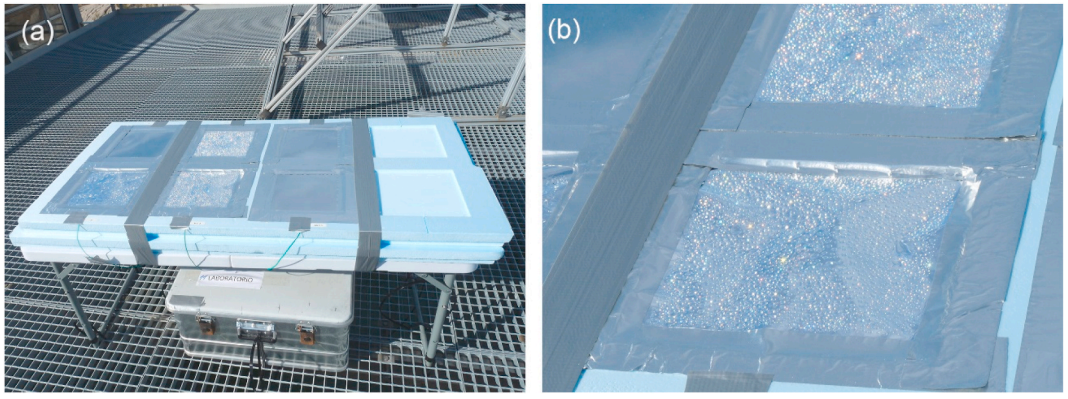


**Fig. 16.** Photos taken Day 4 at 12:12 (a) all the samples in the insulation board, showing condensation in the samples with the plastic substrate (b) the Vikuiti samples with the emissive coating.

than V1, but it was V1 that achieved a more stable lower temperature during all the experiment days except day 1, probably due to low temperatures and high humidity (Fig. 15 (b)). Several significant temperature drops in the AS samples (Fig. 15 (a)) can be explained because of water condensation on the samples' surface before noon. Water condensation augments emissivity, and the evaporation of this layer might lead to some significant temperature decrease due to evaporative cooling. Although the temperature difference is less significant, it can be observed in the Vikuiti samples around noon.

Tables 3-7 summarize the surface's maximum and minimum temperatures, the maximum and minimum difference between surface temperature and ambient temperature for the five consecutive days.

**Table 3**
Summary of the measured surface temperature, data from day 1.

| Day 1 (11:00–24:00) | | | | | | |
|---|---|---|---|---|---|---|
| | A | AS1 | AS2 | V | V1 | V2 |
| Max surface T (°C) ±0.2 °C | 23.2 | 21.6 | 21.9 | 15 | 15 | 13.7 |
| Min surface T (°C) ±0.2 °C | 0.2 | −0.6 | 0.2 | −1.2 | −1.5 | −1.2 |
| ΔT Max ($T_{surf}$-$T_{amb}$) ±0.4 °C | 11.86 | 9.86 | 10.46 | 3.92 | 3.94 | 2.52 |
| ΔT Min ($T_{surf}$-$T_{amb}$) ±0.4 °C | −3.43 | −4.41 | −3.71 | −5.73 | −5.83 | −6.13 |

**Table 4**
Summary of the measured surface temperature, data from day 2.

| Day 2 (00:00–24:00) | | | | | | |
|---|---|---|---|---|---|---|
| | A | AS1 | AS2 | V | V1 | V2 |
| Max surface T (°C) ±0.2 °C | 33.5 | 30.6 | 31.6 | 16.1 | 15.5 | 16.2 |
| Min surface T (°C) ±0.2 °C | 5.3 | 2.8 | 3.8 | 2 | 1.1 | 1.4 |
| ΔT Max ($T_{surf}$-$T_{amb}$) ±0.4 °C | 18.15 | 15.37 | 15.94 | 1.88 | 0.53 | 1.20 |
| ΔT Min ($T_{surf}$-$T_{amb}$) ±0.4 °C | −2.96 | −3.37 | −2.66 | −5.83 | −6.63 | −5.97 |

**Table 5**
Summary of the measured surface temperature, data from day 3.

| Day 3 (00:00–24:00) | | | | | | |
|---|---|---|---|---|---|---|
| | A | AS1 | AS2 | V | V1 | V2 |
| Max surface T (°C) ±0.2 °C | 36.5 | 34.2 | 34.6 | 16.8 | 15.8 | 17.2 |
| Min surface T (°C) ±0.2 °C | 7.6 | 6.4 | 6.6 | 4.1 | 3.1 | 3.3 |
| ΔT Max ($T_{surf}$-$T_{amb}$) ±0.4 °C | 17.47 | 15.17 | 15.21 | 1.28 | −0.10 | 0.43 |
| ΔT Min ($T_{surf}$-$T_{amb}$) ±0.4 °C | −6.49 | −6.63 | −6.63 | −8.23 | −9.13 | −9.13 |

**Table 6**
Summary of the measured surface temperature, data from day 4.

| Day 4 (00:00–24:00) | | | | | | |
|---|---|---|---|---|---|---|
| | A | AS1 | AS2 | V | V1 | V2 |
| Max surface T (°C) ±0.2 °C | 33.4 | 32.1 | 31.6 | 25.3 | 24.2 | 23.5 |
| Min surface T (°C) ±0.2 °C | 17 | 11.9 | 13.2 | 11.5 | 9.7 | 9.9 |
| ΔT Max ($T_{surf}$-$T_{amb}$) ±0.4 °C | 11.23 | 9.93 | 9.43 | 3.75 | 2.55 | 1.84 |
| ΔT Min ($T_{surf}$-$T_{amb}$) ±0.4 °C | −1.36 | −7.21 | −5.91 | −8.31 | −10.11 | −7.21 |

Positive values correspond to materials heating and negative values when materials cool down below ambient temperatures.

### 3.3. Discussion of the results

This research has studied scalable daytime radiative cooling materials in a moderate climate throughout different meteorological conditions far from the usual experiments done under ideal settings (no convection and low relative humidity). This study presents the simulation, development, characterization, and testing of two kinds of daytime radiative cooling materials based on silica-derived emissive layers. The material design and simulation proved to be a valuable tool while leading to an in-depth understanding of the structures' optical behavior. The optimization provided the necessary insight regarding the adequate material's thickness and validated the proposed structures before fabrication. The sprayable emissive coating is a highly versatile solution for plastic and metallic applications; it is transparent in the solar wavelengths leaving the substrate exposed; thus, the final material's solar reflectivity depends on the substrate of application. Two kinds of reflective layers were selected, aluminum substrate and commercial Vikuiti. The simulations and the finally employed materials differ due to limitations in the fabrication process. Since the bare aluminum substrate's reflectivity is lower than developed materials that were neither very solar reflective nor very emissive in the atmospheric window, another substrate was selected to improve the solar wavelengths' reflectivity Vikuiti. As a result, a new formulation for plastic applications was developed. Their reflectivity, gloss, adherence, among others, were characterized.

**Table 7**
Summary of measured surface temperature, data from day 5.

| Day 5 (00:00–09:25) | | | | | | |
|---|---|---|---|---|---|---|
| | A | AS1 | AS2 | V | V1 | V2 |
| Max surface T (°C) ±0.2 °C | 18.2 | 17.9 | 17.9 | 17.2 | 16.8 | 17.3 |
| Min surface T (°C) ±0.2 °C | 12.9 | 12.7 | 13 | 13.1 | 13 | 12.9 |
| ΔT Max ($T_{surf}$-$T_{amb}$) ±0.4 °C | 0.84 | 0.55 | 0.55 | 0.29 | −0.45 | −0.06 |
| ΔT Min ($T_{surf}$-$T_{amb}$) ±0.4 °C | −3.40 | −3.57 | −3.40 | −3.31 | −3.81 | −3.70 |

The metallic samples resulted in spectrally selective daytime radiative cooling (DTRC) materials in the atmospheric window, and the plastic samples were broadband emitters. The experiment presents a comprehensive overview of their true potential throughout different meteorological conditions, wind speed, humidity, temperature, and ambient radiation. The materials with a highly reflective substrate such as Vikuiti can achieve subambient cooling during the day, however under high ambient radiation and relative humidity perform poorly; therefore, strict selectivity is desired. The more strictly selective materials based on aluminum (AS) are absorbent in the first atmospheric window (8–13 μm); thus, the effect of the second atmospheric window (16–25 μm) is negligible. The V and VS samples are broadband emitters, and any received longwave radiation will affect them by increasing the thermal balance temperature. In this case, the second atmospheric window will have a more significant impact. Both atmospheric windows are affected by humidity, affecting more the broadband materials. Although the samples with the metallic substrate are above ambient air temperature throughout most of the daytime, the addition of an emissive layer improves its emissivity considerably and, therefore, its thermal behavior during the day, compared to the substrate.

The spray deposition used in this research presents two main advantages: speed and scalability. Drawbacks from this technique are thickness control and replicability. Deposition with this fabrication technique should be further studied. As mentioned before, the thicknesses could not be controlled as desired, leading to two consequences. First, every time a deposition is made, the thickness will be different, leading to a replicability problem. Secondly, the spray coating is done manually, leading to heterogeneous deposition in the samples. Concluding, the deposition method needs substantial changes, with a more mechanical and controlled process. It is essential to control both the application homogeneity and thickness without compromising the ability to scale the samples' size.

The experiment took place in Sarriguren, 8 km away from Pamplona during five consecutive fall days (16th to October 20, 2020); according to the Köppen-Geiger classification, it is a Cfb climate. To test the emissive coating's efficiency, the samples without the coatings were tested alongside bare aluminum and one Vikuiti film (A and V). The

Vikuiti based samples V, V1 and V2 dropped their temperature during daytime (12:00–15:00) an average of 1 °C, 2.05 °C and 2.70 °C below ambient, respectively, and a maximum of 6.26 °C, 7.45 °C and, 7.97 °C. The samples with the aluminum substrate did not reach subambient cooling during the entire day; however, the temperature of the emissive coating samples was below the temperature of the bare aluminum substrate, a mean of 1.88 °C (AS1) and 1.16 °C (AS2). All the samples achieved nighttime radiative cooling since they were emissive in the atmospheric window. The samples made of aluminum plus the emissive coating achieved a 1.88 °C reduction compared to the bare aluminum and a maximum temperature difference of 11.2 °C (Day 3 at 12:55).

Other radiative cooling materials have been tested and proven subambient temperatures, but either the relative humidity was lower, or a convection barrier protected the samples, and in some instances, the sun was blocked with sun shading devices. Raman et al. photonic structure reported a 4.9 K below ambient in Stanford; the sample was protected with a polyethylene cover to eliminate convection [13]. Radiative cooling materials based on $TiO_2$, $SiO_2$, and SiC nanoparticles were tested in Shanghai, Cfa climate humid subtropical. However, the materials did not achieve subambient temperatures during the day due to high relative humidity (50–70%) [15]. Another test compared, in the same location, twelve samples of $SiO_2$ (TPX) hybrid system deposited on fluorine-doped tin oxide (FTO) substrates, showing an average temperature of 15 °C higher than ambient even with a convection barrier [58]. A multilayer photonic material based on $TiO_2$ and $SiO_2$ reported a 7.3 °C subambient temperature at noontime in Beijing with exceeding solar radiation of 430 W $m^{-2}$ and relative humidity between 50 and 90%.That material had a low-density polyethylene as a wind cover [27], and a sun shading device was used. The results presented in this study show a promising path in using PMSQ (polymethylsilsesquioxane) with silica nanoparticles as an emissive coating for radiative cooling under various meteorological conditions, where other experiments and materials failed to achieve subambient cooling. The Vikuiti samples with the emissive coating achieved temperature reductions up to 7.97 °C. Moreover, the easy deposition technique and the possibility to apply onto other substrates present a great candidate for scalable daytime radiative cooling. Finally, the materials were tested under non-favorable conditions, without sun shading devices nor convective shields, achieving substantial temperature drops. The results presented open an interesting research line for future application in the built environment.

## 4. Conclusions

This research has studied scalable daytime radiative cooling materials in a moderate climate throughout different meteorological conditions far from the usual experiments done under real conditions and ideal setting (minimizing convection and relative humidity). This study presents the simulation, development, characterization, and testing of two kinds of daytime radiative cooling materials based on silica derived emissive layers. The material design and simulation helped understand the structures' optical behavior, providing the necessary insight to tailor the material's thickness and validate the proposed structures before manufacturing.

We have proved, for the first time to our knowledge, that low cost (0.3 €/$m^2$ for a layer of 2 μm of PMSQ and $SiO_2$ particles), scalable and sprayable coatings provide significant radiative cooling, as to reduce its temperature significantly over bare substrates in real climatic conditions.

The following conclusions can be obtained:

(1) Under most climatic conditions, the materials have the ability to cool down a metallic substrate a mean of at least 1.7 °C with up to 12 °C temperature drops.
(2) The samples based on the Vikuiti substrate dropped their temperature during the highest solar radiation and maximum ambient temperatures, an average of 2.70 °C below ambient and a maximum 7.97 °C during the day.
(3) The materials developed, in both cases, have better thermal behavior than the substrates without treatment (enhanced solar reflector ESR and aluminum).
(4) Although the materials' spectra were not ideal 0.7 (solar reflectivity) and 0.34 (emissivity in the AW), the materials could stay below the ambient temperature at least until noon.
(5) The cost and deposition system presented are good candidates for future broad application in the built environment and architecture.

The path has proven promising for future scalable material development. Further testing on sprayed coating techniques should be made:

(1) Applicating on different substrates present in the built environment (e.g., concrete, ceramic, and glass). The potential substrates need to have sky access to evacuate heat—especially important applications in roofs and other exposed horizontal building surfaces.
(2) Testing under different meteorological conditions to determine the ideal material for each climate and application.
(3) Incorporating low-cost switchable technologies to avoid overcooling during the heating seasons.
(4) Studying their degradation and aging as they will be exposed to extreme weather conditions and prolonged periods.

These new scalable polymeric materials could lower the cooling demands of buildings and alleviate heat buildup in cities, aiding to lowering the Urban Heat Island phenomenon. Moreover, the technique might be of significant interest for building retrofitting as a spraying technique can be applied onsite or as industrialized elements.

## Contribution

Laura Carlosena, investigation, conceptualization, methodology, data curation, formal analysis, and writing original draft; Ángel Andueza, validation and software, writing, reviewing, and editing; Luis Torres, data curation, reviewing and editing; Olatz Irulegi, reviewing and editing, supervision; Rufino Hernández, supervision and funding acquisition; Joaquín Sevilla, writing, reviewing, and editing; Mattheos Santamouris, writing, reviewing and editing, supervision.

## Funding

The materials development in this research received a grant from the Government of Navarre "Convocatoria proyectos I + D 2019" file number 0011-1365-2019-000051; and financial support from Alonso Hernández & asociados arquitectura, S. L.

## CRediT authorship contribution statement

**Laura Carlosena:** Investigation, Conceptualization, Methodology, Data curation, Formal analysis, and, Writing – original draft. **Ángel Andueza:** Validation, and, Software, Writing – review & editing. **Luis Torres:** Data curation, Writing – review & editing. **Olatz Irulegi:** Writing – review & editing, Supervision. **Rufino J. Hernández-Minguillón:** Supervision, and, Funding acquisition. **Joaquín Sevilla:** Writing – review & editing. **Mattheos Santamouris:** Writing – review & editing, Supervision.

## Declaration of competing interest

The authors declare that they have no known competing financial interests or personal relationships that could have appeared to influence the work reported in this paper.

## Acknowledgment

The authors would like to thank Dr. Jaione Bengoechea and acknowledge the National Renewable Energy Center (CENER) for allowing the use of their rooftop facilities for the experimental setup.

## References

[1] H. Akbari, C. Cartalis, D. Kolokotsa, A. Muscio, A.L. Pisello, F. Rossi, M. Santamouris, A. Synnef, N.H. Wong, M. Zinzi, Local climate change and urban heat island mitigation techniques – the state of the art, J. Civ. Eng. Manag. 22 (2016) 1–16, https://doi.org/10.3846/13923730.2015.1111934.

[2] M. Santamouris, Analyzing the heat island magnitude and characteristics in one hundred Asian and Australian cities and regions, Sci. Total Environ. 512–513 (2015) 582–598, https://doi.org/10.1016/j.scitotenv.2015.01.060.

[3] M. Santamouris, Regulating the damaged thermostat of the cities—status, impacts and mitigation challenges, Energy Build. 91 (2015) 43–56, https://doi.org/10.1016/j.enbuild.2015.01.027.

[4] D. Founda, M. Santamouris, Synergies between urban heat island and heat waves in athens (Greece), during an extremely hot summer, Sci. Rep. 7 (2017) (2012), https://doi.org/10.1038/s41598-017-11407-6.

[5] M. Santamouris, Recent progress on urban overheating and heat island research. Integrated assessment of the energy, environmental, vulnerability and health impact. Synergies with the global climate change, Energy Build. 207 (2020) 109482, https://doi.org/10.1016/j.enbuild.2019.109482.

[6] M. Santamouris, C. Cartalis, A. Synnefa, D. Kolokotsa, On the impact of urban heat island and global warming on the power demand and electricity consumption of buildings—a review, Energy Build. 98 (2015) 119–124, https://doi.org/10.1016/j.enbuild.2014.09.052.

[7] M. Santamouris, On the energy impact of urban heat island and global warming on buildings, Energy Build. 82 (2014) 100–113, https://doi.org/10.1016/j.enbuild.2014.07.022.

[8] L.H. Schinasi, T. Benmarhnia, A.J. De Roos, Modification of the association between high ambient temperature and health by urban microclimate indicators: a systematic review and meta-analysis, Environ. Res. 161 (2018) 168–180, https://doi.org/10.1016/j.envres.2017.11.004.

[9] M. Santamouris, L. Ding, F. Fiorito, P. Oldfield, P. Osmond, R. Paolini, D. Prasad, A. Synnefa, Passive and active cooling for the outdoor built environment – analysis and assessment of the cooling potential of mitigation technologies using performance data from 220 large scale projects, Sol. Energy 154 (2016) 14–33, https://doi.org/10.1016/j.solener.2016.12.006.

[10] M. Santamouris, G.Y. Yun, Recent development and research priorities on cool and super cool materials to mitigate urban heat island, Renew. Energy 161 (2020) 792–807, https://doi.org/10.1016/j.renene.2020.07.109.

[11] M. Santamouris, F. Fiorito, On the impact of modified urban albedo on ambient temperature and heat related mortality, Sol. Energy 216 (2021) 493–507, https://doi.org/10.1016/j.solener.2021.01.031.

[12] M. Santamouris, J. Feng, Recent progress in daytime radiative cooling: is it the air conditioner of the future? Buildings 8 (2018) 168, https://doi.org/10.3390/buildings8120168.

[13] A.P. Raman, M.A. Anoma, L. Zhu, E. Rephaeli, S. Fan, Passive radiative cooling below ambient air temperature under direct sunlight, Nature 515 (2014) 540–544, https://doi.org/10.1038/nature13883.

[14] Z. Chen, L. Zhu, A. Raman, S. Fan, Radiative cooling to deep sub-freezing temperatures through a 24-h day–night cycle, Nat. Commun. 7 (2016) 13729, https://doi.org/10.1038/ncomms13729.

[15] H. Bao, C. Yan, B. Wang, X. Fang, C.Y. Zhao, X. Ruan, Double-layer nanoparticle-based coatings for efficient terrestrial radiative cooling, Sol. Energy Mater. Sol. Cells 168 (2017) 78–84, https://doi.org/10.1016/j.solmat.2017.04.020.

[16] J. Kou, Z. Jurado, Z. Chen, S. Fan, A.J. Minnich, Daytime radiative cooling using near-black infrared emitters, ACS Photonics 4 (2017) 626–630, https://doi.org/10.1021/acsphotonics.6b00991.

[17] M.A. Kecebas, M.P. Menguc, A. Kosar, K. Sendur, Passive radiative cooling design with broadband optical thin-film filters, J. Quant. Spectrosc. Radiat. Transf. 198 (2017) 179–186, https://doi.org/10.1016/j.jqsrt.2017.03.046.

[18] A. Hervé, J. Drévillon, Y. Ezzahri, K. Joulain, Radiative cooling by tailoring surfaces with microstructures: association of a grating and a multi-layer structure, J. Quant. Spectrosc. Radiat. Transf. 221 (2018) 155–163, https://doi.org/10.1016/j.jqsrt.2018.09.015.

[19] E. Rephaeli, A. Raman, S. Fan, Ultrabroadband photonic structures to achieve high-performance daytime radiative cooling, Nano Lett. 13 (2013), https://doi.org/10.1021/nl4004283, 130311121615001.

[20] M.M. Hossain, B. Jia, M. Gu, A metamaterial emitter for highly efficient radiative cooling, Adv. Opt. Mater. 3 (2015) 1047–1051, https://doi.org/10.1002/adom.201500119.

[21] C. Zou, G. Ren, M.M. Hossain, S. Nirantar, W. Withayachumnankul, T. Ahmed, M. Bhaskaran, S. Sriram, M. Gu, C. Fumeaux, Metal-loaded dielectric resonator metasurfaces for radiative cooling, Adv. Opt. Mater. 5 (2017) 1700460, https://doi.org/10.1002/adom.201700460.

[22] A.R. Gentle, G.B. Smith, Radiative heat pumping from the earth using surface phonon resonant nanoparticles, Nano Lett. 10 (2010) 373–379, https://doi.org/10.1021/nl903271d.

[23] Y. Zhai, Y. Ma, S.N. David, D. Zhao, R. Lou, G. Tan, R. Yang, X. Yin, Scalable-manufactured randomized glass-polymer hybrid metamaterial for daytime radiative cooling, Science 355 (2017) 1062–1066, https://doi.org/10.1126/science.aai7899.

[24] Z. Yi, Y. lv, D. Xu, J. Xu, H. Qian, D. Zhao, R. Yang, A transparent radiative cooling film for building energy saving, Energy Built Environ (2020), https://doi.org/10.1016/j.enbenv.2020.07.003.

[25] Z. Huang, X. Ruan, Nanoparticle embedded double-layer coating for daytime radiative cooling, Int. J. Heat Mass Tran. 104 (2017) 890–896, https://doi.org/10.1016/j.ijheatmasstransfer.2016.08.009.

[26] J. Mandal, Y. Fu, A. Overvig, M. Jia, K. Sun, N. Shi, H. Zhou, X. Xiao, N. Yu, Y. Yang, Hierarchically porous polymer coatings for highly efficient passive daytime radiative cooling, Science (2018), https://doi.org/10.1126/science.aat9513 eaat9513.

[27] X. Ao, M. Hu, B. Zhao, N. Chen, G. Pei, C. Zou, Preliminary experimental study of a specular and a diffuse surface for daytime radiative cooling, Sol. Energy Mater. Sol. Cells 191 (2019) 290–296, https://doi.org/10.1016/j.solmat.2018.11.032.

[28] G.B. Smith, Amplified radiative cooling via optimised combinations of aperture geometry and spectral emittance profiles of surfaces and the atmosphere, Sol. Energy Mater. Sol. Cells 93 (2009) 1696–1701, https://doi.org/10.1016/j.solmat.2009.05.015.

[29] D. Aviv, F. Meggers, Cooling oculus for desert climate-dynamic structure for evaporative downdraft and night sky cooling, Energy Procedia, Lausanne, Switzerland, 2017, pp. 1124–1129, https://doi.org/10.1016/j.egypro.2017.07.474.

[30] L. Zhou, H. Song, J. Liang, M. Singer, M. Zhou, E. Stegenburgs, N. Zhang, T.K. Ng, Z. Yu, B. Ooi, Q. Gan, All-day radiative cooling using beam-controlled architectures, in: Conf. Lasers Electro-Opt. 2019 Pap. ATh1I2, Optical Society of America, 2019, https://doi.org/10.1364/CLEO_AT.2019.ATh1I.2. ATh1I.2.

[31] L. Zhou, H. Song, J. Liang, M. Singer, M. Zhou, E. Stegenburgs, N. Zhang, C. Xu, T. Ng, Z. Yu, B. Ooi, Q. Gan, A polydimethylsiloxane-coated metal structure for all-day radiative cooling, Nat. Sustain. 2 (2019) 718–724, https://doi.org/10.1038/s41893-019-0348-5.

[32] A. Ahmadi, M.A. Karaei, H. Fallah, Investigation of night (radiative) cooling event and construction of experimental radiator, Int. J. Adv. Biotechnol. Res. 7 (2016) 1180–1184.

[33] E. Erell, Y. Etzion, A radiative cooling system using water as a heat exchange medium, Architect. Sci. Rev. 35 (1992) 39–49, https://doi.org/10.1080/00038628.1992.9696712.

[34] E. Erell, Y. Etzion, Analysis and experimental verification of an improved cooling radiator, Renew. Energy 16 (1999) 700–703, https://doi.org/10.1016/S0960-1481(98)00255-9.

[35] M.G. Meir, J.B. Rekstad, O.M. LØvvik, A study of a polymer-based radiative cooling system, Sol. Energy 73 (2002) 403–417.

[36] E. Hosseinzadeh, H. Taherian, An experimental and analytical study of a radiative cooling system with unglazed flat plate collectors, Int. J. Green Energy 9 (2012) 766–779, https://doi.org/10.1080/15435075.2011.641189.

[37] J.A. Ferrer Tevar, S. Castaño, A. Garrido Marijuán, M.R. Heras, J. Pistono, Modelling and experimental analysis of three radioconvective panels for night cooling, Energy Build. 107 (2015) 37–48, https://doi.org/10.1016/j.enbuild.2015.07.027.

[38] D. Zhao, C.E. Martini, S. Jiang, Y. Ma, Y. Zhai, G. Tan, X. Yin, R. Yang, Development of a single-phase thermosiphon for cold collection and storage of radiative cooling, Appl. Energy 205 (2017) 1260–1269, https://doi.org/10.1016/j.apenergy.2017.08.057.

[39] E.A. Goldstein, A.P. Raman, S. Fan, Sub-ambient non-evaporative fluid cooling with the sky, Nat. Energy. 2 (2017), nenergy2017143, https://doi.org/10.1038/nenergy.2017.143.

[40] X. Lu, P. Xu, H. Wang, T. Yang, J. Hou, Cooling potential and applications prospects of passive radiative cooling in buildings: the current state-of-the-art, Renew. Sustain. Energy Rev. 65 (2016) 1079–1097, https://doi.org/10.1016/j.rser.2016.07.058.

[41] P. Berdahl, M. Martin, F. Sakkal, Thermal performance of radiative cooling panels, Int. J. Heat Mass Tran. 26 (1983) 871–880, https://doi.org/10.1016/S0017-9310(83)80111-2.

[42] B. Landro, P.G. McCormick, Effect of surface characteristics and atmospheric conditions on radiative heat loss to a clear sky, Int. J. Heat Mass Tran. 23 (1980) 613–620, https://doi.org/10.1016/0017-9310(80)90004-6.

[43] M. Matsuta, S. Terada, H. Ito, Solar heating and radiative cooling using a solar collector-sky radiator with a spectrally selective surface, Sol. Energy 39 (1987) 183–186, https://doi.org/10.1016/S0038-092X(87)80026-9.

[44] A.H.H. Ali, H. Saito, I.M.S. Taha, K. Kishinami, I.M. Ismail, Effect of aging, thickness and color on both the radiative properties of polyethylene films and performance of the nocturnal cooling unit, Energy Convers. Manag. 39 (1998) 87–93, https://doi.org/10.1016/S0196-8904(96)00174-4.

[45] A.R. Gentle, G. Smith, Performance comparisons of sky window spectral selective and high emittance radiant cooling systems under varying atmospheric conditions, in: Canberra, ACT, Australia, 2010. https://opus.lib.uts.edu.au/handle/10453/19359. (Accessed 12 June 2019). accessed.

[46] L. Carlosena, Á. Ruiz-Pardo, J. Feng, O. Irulegi, R.J. Hernández-Minguillón, M. Santamouris, On the energy potential of daytime radiative cooling for urban heat island mitigation, Sol. Energy 208 (2020) 430–444, https://doi.org/10.1016/j.solener.2020.08.015.

[47] Cst Studio Suite, Simulia (2018).

[48] T.S. Eriksson, S.-J. Jiang, C.G. Granqvist, Surface coatings for radiative cooling applications: silicon dioxide and silicon nitride made by reactive rf-sputtering, Sol. Energy Mater. 12 (1985) 319–325, https://doi.org/10.1016/0165-1633(85)90001-2.

[49] C.G. Granqvist, A. Hjortsberg, Radiative cooling to low temperatures: general considerations and application to selectively emitting SiO films, J. Appl. Phys. 52 (1981) 4205–4220, https://doi.org/10.1063/1.329270.
[50] M. Clemens, T. Weiland, Discrete electromagnetism with the finite integration technique - abstract, J. Electromagn. Waves Appl. 15 (2001) 79–80, https://doi.org/10.1163/156939301X00661.
[51] K.C. Johnson, GD-calc, KJ Innov, 2005. https://kjinnovation.com/. (Accessed 5 December 2020). accessed.
[52] M.G. Moharam, T.K. Gaylord, Rigorous coupled-wave analysis of planar-grating diffraction, JOSA 71 (1981) 811–818, https://doi.org/10.1364/JOSA.71.000811.
[53] J. Gjessing, Photonic Crystals for Light Trapping in Solar Cells, University of Oslo, 2011. https://www.mn.uio.no/its/english/people/aca/aas/theses/JoGjessing_PhD_thesis_final16feb2012.pdf. (Accessed 5 December 2020). accessed.
[54] 3MTM enhanced specular reflector (3M ESR) | 3M United States (n.d.), https://www.3m.com/3M/en_US/company-us/all-3m-products/~/3M-Enhanced-Specular-Reflector-3M-ESR-/?N=5002385+3293061534&rt=rud. (Accessed 8 September 2020). accessed.
[55] A.R. Gentle, G.B. Smith, A subambient open roof surface under the mid-summer sun, Adv. Sci. 2 (2015), https://doi.org/10.1002/advs.201500119.
[56] M. Fabian, E. Lewis, T. Newe, S. Lochmann, Optical fibre cavity for ring-down experiments with low coupling losses, Meas. Sci. Technol. 21 (2010), 094034, https://doi.org/10.1088/0957-0233/21/9/094034.
[57] J. Feng, K. Gao, M. Santamouris, K.W. Shah, G. Ranzi, Dynamic impact of climate on the performance of daytime radiative cooling materials, Sol. Energy Mater. Sol. Cells 208 (2020) 110426, https://doi.org/10.1016/j.solmat.2020.110426.
[58] J. Yang, X. Gao, Y. Wu, T. Zhang, H. Zeng, X. Li, Nanoporous silica microspheres–ploymethylpentene (TPX) hybrid films toward effective daytime radiative cooling, Sol. Energy Mater. Sol. Cells 206 (2020) 110301, https://doi.org/10.1016/j.solmat.2019.110301.